Detection, mitigation and isolation of Galileo interferers

Anne Ferreol *Thales communications.*
Philippe Morgand, *Thales communications*
Eugenio Rossini, *Space Engineering*

I. BIOGRAPHY

The MAGIC (MAnagement of Galileo Interference and Counter measures) proposal has been realized in order to answer to the call for tender "GJU call 2416".
This European project proposed with the participation of Space Engineering (I), Thales Communications (F), Joanneum Research (A), Teletel (Gr), University of Bologna (I) and France Developpement Conseil (F) was selected in August 2005. MAGIC started in November 2005 for a 24 months duration is today finalized.

II. INTRODUCTION

This paper describes the activities carried out in the framework of the MAGIC (MAnagement of Galileo Interference and Counter measures) project, a GSA European project aimed at analyzing the potential interfering scenarios for the Galileo signals. In particular the main tasks of the project include the study of suitable detection, localization and mitigation strategies to be implemented in a dedicated test bed in order to validate it with trials on site on synthetic or real existing interferers. The MAGIC test bed realized during the project prefigures an Interferer Observation System (IOS) that allow the detection, classification, mitigation and direction of arrival estimation of the interferer waves.
In addition, an interferer campaign of measurement and analysis conducted by JR was realized over parts of four European countries as Austria, Italy, France and Germany.
Finally, the MAGIC project allowed the study and definition of the typical implementation of a GIMS (Galileo Interferer Measurement System) infrastructure based upon Interference Observation Sites (IOS) and Interference Control Centres (ICC).
These local components are in charged of integrating, processing observations and disseminating the relevant results. The GIMS can be installed in typical areas as airports and harbours where it can be put side by side to already existing LAA (Local Area Augmentation) improving their availability through protecting the DAT (Differential Augmentation Terminals) against the interferences. The results achieved during these different items are shown in this article.

III. INTERFERENCE DETECTION SIMULATIONS

The detection schema adopted in the MAGIC Project is shown in Figure 1.

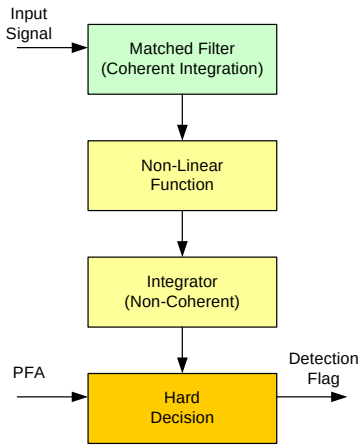

Figure 1 – Detection Schema

The second and third stages after the matched filter carry out the energy integration of the input samples. The last stage is a hard decision logic, which raises a detection flag when the input is above a threshold. The threshold is computed on the basis of the Probability of False Alarm (PFA) established by the user. A calibration phase is foreseen to estimate the noise power and to provide a criterion to create a threshold mechanism.
The non-linear function has been implemented subdividing the signal to be detected into a given number of frequency bins and then, for each of them, extracting its energy together to its Probability of Detection (PD). The PD is then compared with a threshold obtained from the PFA.
A simulation analysis has been carried out using as input different potential interfering signals immersed in Gaussian noise: CW, Sweeps and Pulsed Signals. The behaviour of the algorithms has been tested extracting the Receiver Operating Characteristic (ROC) where the response of each bin is plotted in a PFA against PD diagram.
After the detection, several classification algorithms have been studied and implemented. To summarise the detection and classification processing it is possible to take as reference the flow diagram shown in Figure 2.

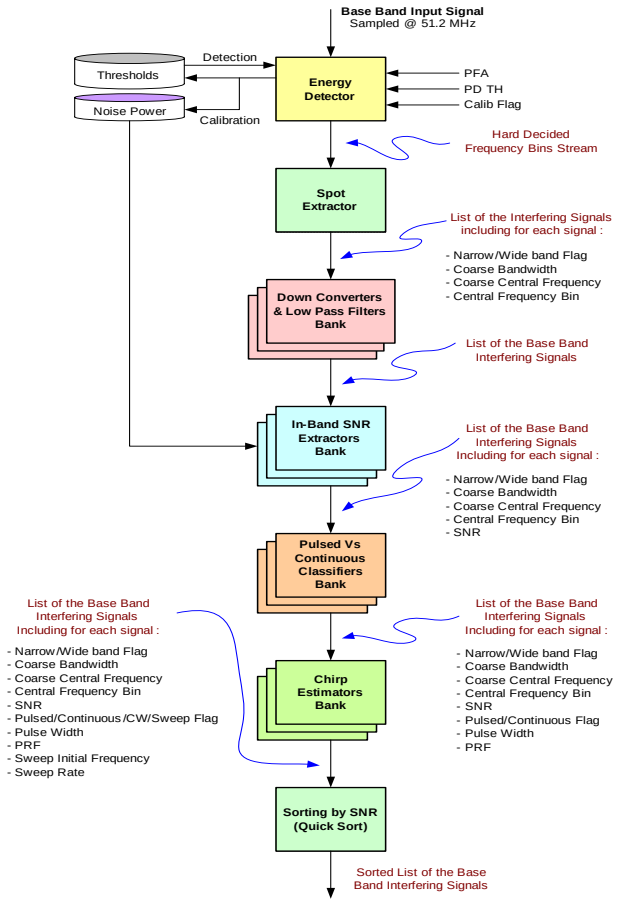

Figure 2 – Detection and Classification Flow

After the energy detector the signal is subdivided into frequency bins, which are arranged in spots when they are adjacent. The so obtained spots correspond to several, spectrally separated, interfering signals, which must be processed separately from this point on.

The signal, after the spot extractor, appears as a list of records where each record includes the coarse bandwidth (BW) and the coarse central frequency (CF) of a given interfering signal. A bank of Low Pass Filters with bandwidth BW is then applied, after a down conversion at central frequency CF, to obtain a separate signal for each spot (i.e. for each interfering signal).

The next algorithms (SNR extractor, pulsed signal classifier and chirp estimator) add further details to each record, which are useful to identify the type of the signal.

Finally the list of detected interfering signals is sorted by SNR in order to provide an output, which can be easily used to select the most threatening interferences to be mitigated.

The continuous versus pulsed classification is carried out for each spot (i.e. for each interfering signal identified by the spot extractor). Several signals are processed sequentially using an algorithm based on the Time Of Arrival (TOA) of the rising and falling edge of the pulses. The algorithm employed provides the PW and the PRF of the pulsed signals.

The adopted approach used to estimate the frequency and frequency rate of a chirp signal is a FFT based algorithm. The Observation Time (T_{obs}) time interval is divided into 16 sub slots at the beginning of which a 2^{16} points FFT is performed. The frequency corresponding to the maximum modulus of each FFT is extracted and used to classify the signal according to the following rules: (i) if the frequencies corresponding to the maximum modulus of the FFTs are monotonically increasing or monotonically decreasing the signal is classified as a sweep; (ii) if the variance of the frequencies corresponding to the maximum modulus of the FFTs is less than a given threshold the signal is classified as CW; (iii) if the previous two conditions are not satisfied the signal is classified as unknown. This algorithm concludes the detection and classification processing.

To have an idea of the performances obtained with this processing it is possible to look at the Figure 3 where a typical interference scenario is shown. The scenario includes four CWs at central frequencies -20.5 MHz, -17 MHz, 20 MHz and 23 MHz; two sweeps with start frequencies -10.4 MHz and 3.9 MHz and frequency rates 5.1 MHz/sec and -17.3 MHz/sec respectively, and finally a pulsed signal at central frequency 10.4 MHz having a PRF of 2.7 KHz and a pulse width of 3.5 µsec.

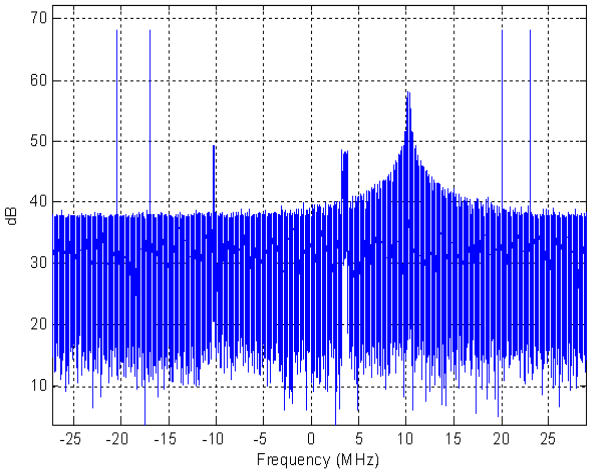

Figure 3 – Typical Interference Scenario

The implemented set of algorithms described above successfully detected each interfering signal present in this scenario and correctly classified them according to their characteristics.

IV. INTERFERENCE MITIGATION SIMULATIONS

Once interference has been detected and isolated, an interference mitigation strategy can be put in force. In the MAGIC Project two different mitigation techniques have been implemented: (i) a Frequency Domain Interference Mitigation (FDIM), (ii) a Spatial Domain Interference Mitigation (SDIM), , (iii) Joint Time-Frequency Domain Interference Mitigation (TFDIM), (iv) Joint Space-Time-Frequency Domain Interference Mitigation (STFDIM). Among them the first two techniques are detailed in this paper..

An example of the SDIM pattern after the steering is given in the Figure 4.

The position of a null in the antenna pattern virtually sets to zero the power received from that precise direction so, if the Direction Of Arrival (DOA) estimation of the interfering signals is precise enough, the attenuation of the interference may be very strong. Naturally errors in the estimation have to be considered, so the cancellation

will never be total. It is possible to widen the tolerance in azimuth by imposing several near nulls.

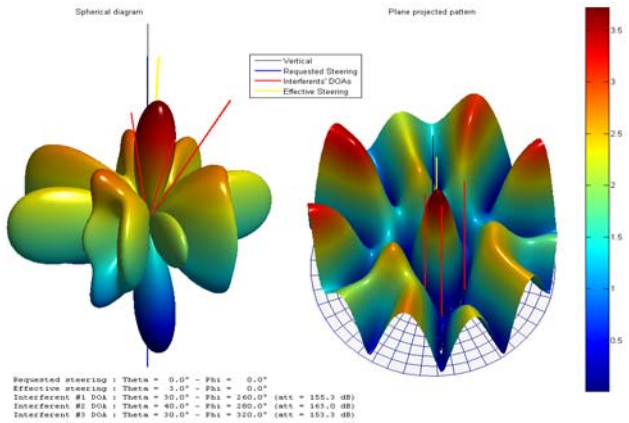

Figure 4 – SDIM: Steered Pattern

Another interesting aspect of the algorithm is connected with the hypothesis that the carrier frequency is large compared to the bandwidth of the impinging signal, so that the modulating signal may be treated as quasi-static during time intervals. This means that, if the signal bandwidth is not so small, the delay is perceptible also on the information-carrying signal, and the overall mitigation effort is smaller.

The performance of the space-domain mitigation algorithm can be presented in terms of BER. The red BER curve in Figure 5 is the theoretical limit and the blue ones are the measured curves under different INR.

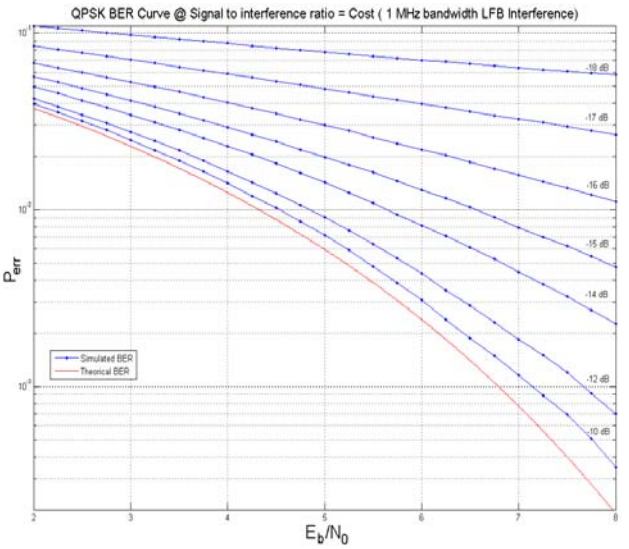

Figure 5 – SDIM BER Curve

The approach of the FDIM technique consists in taking the Fourier transform of the disturbed signal and in applying to this an adaptive mask in order to notch out the disturbing frequency bins. After that the processing applies an inverse Fourier transformation to bring back the signal to the time domain.

The energy of the Narrow Band Interferer (NBI) is concentrated over a narrow band compared to the band of the Spread Spectrum (SS) signal. Hence in frequency domain its magnitude response presents some peaks, which are much higher than that of SS signal. So the position and magnitude of these peaks can be detected via an envelope detector, so to determine a threshold to reduce the magnitude value of the NBI according to some criterion. The threshold is often close to the magnitude response of the SS signal and it is considered that the frequency bins that excess such threshold contain interference. After reducing the magnitude values of these cells, the most energy of the NBI is cut out, that is, the NBI is suppressed. In Figure 6 a mathematic model for the mitigation technique is shown.

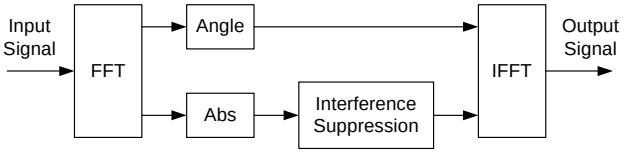

Figure 6 – FDIM Mathematic Model

To make the threshold adaptive, it is determined according to the mean value of the cell energy of a few times current FFT results. Three types of interferences have been considered: a continuous wave, a sweep and a pulsed.

As it was expectable the algorithm best performs in the case of a CW (or very narrow band) interference, since the affected bin is totally masked and the effect on the information signal is almost negligible.

When enlarging the interference band the performance goes rapidly down. This is due to the fact that the more frequency bins are affected by interference (and thus excised), the more quantity of information goes lost.

V. INTERFERENCE ISOLATION SIMULATIONS

The purpose of this section is to describe a location technique of M transmitters (or interferences) located at $\mathbf{E}_m$ $(1 \le m \le M)$ in presence of P reflectors located at $\mathbf{R}_p$ $(1 \le p \le P)$ by the use of multiple AOA (Angles of Arrival) stations located at (**A**,**B**,**C**,…). Figure 7 illustrates the field of propagation between transmitters and AOA stations. Thus, the location and AOA algorithms must take into account multi-sources and multi-paths contexts. Finally the isolation technique gives the location of transmitters (or interferences) and reflectors in $\mathbf{E}_m$ and $\mathbf{R}_p$ respectively.

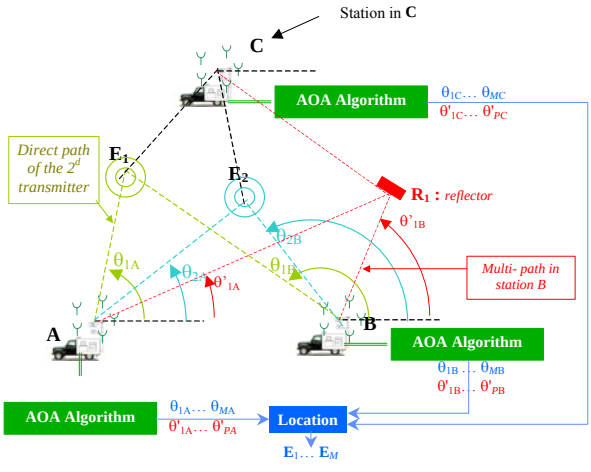

Figure 7- Field of Propagation between the transmitters and the AOA stations

More precisely for the AOA station located at **A,** the angle of arrival of the *m*-th transmitter is noted by θ_{mA} and the one of *p*-th reflector is noted by θ'_{pA}. Similarly the stations **B** and **C** see the *m*-th transmitter at θ_{mB} and θ_{mC} respectively and the *p*-th reflector at θ'_{pB} and θ'_{pC} respectively. The isolation technique needs two steps

- **AOA Algorithm** : Estimation of the AOAs $(\theta_{mA}, \theta'_{pA})$, $(\theta_{mB}, \theta'_{pB})$, $(\theta_{mC}, \theta'_{pC})$,… at the output of each AOA station.
- **Location Algorithm** : Estimation of the location $\mathbf{E}_m$ and $\mathbf{R}_p$ from the AOAs previously estimated. For instance, the location $\mathbf{E}_m$ of the *m*-th transmitter is estimated from angles (θ_{mA}, θ_{mB}, θ_{mC}..).

The following figure shows that the location of more than one source (Transmitters and reflectors) needs at least the use of 3 AOA stations.

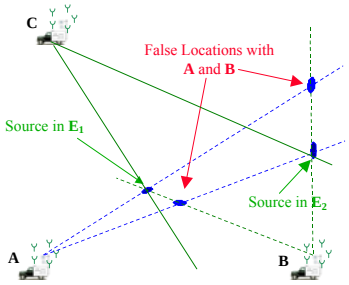

Figure 8- False locations in presence of 2 stations and 2 sources

Figure 8 shows that the location algorithm in presence of 2 sources with the stations **A** and **B** gives 4 locations with 2 true locations and 2 false. These ambiguities can be avoided with the presence of an additional station in **C** because the false location associated to **A** and **C** (or **B** and **C**) are not located at the same place.

AOA algorithm on station A

Each AOA stations are composed by multi-antennas receiver system: The array of antennas is connected to synchronous multi-receivers installed into a vehicle. In Figure 9, the array is horizontal and circular with radius *R* and *N*=5 antennas. The array is at the top of a mast and the elementary antenna is a vertical dipole.

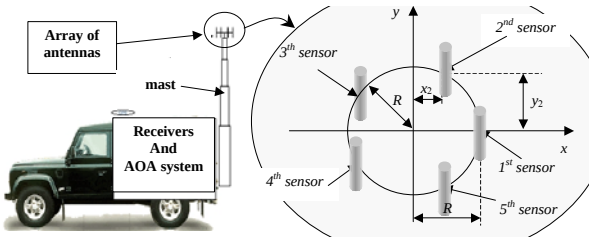

Figure 9- AOA station : Array of antennas and receivers

The AOA technique in each station is identical and the description of this section is focused on station **A**. According to the field of propagation represented in Figure 7, the AOA algorithm must be adapted to multi-sources and multi-paths contexts. This is the reason why High Resolution (HR) algorithms such as [15] -[18] are adapted to this propagation context. The main advantage is that the technique is asymptotically unbiased. More precisely the algorithm depends on multi-paths characteristics:

- **The coherent case** : The time difference of arrival between direct-path and multi-path is neglected to the inverse of the transmitter bandwidth. This last condition has the following mathematical expression:

$$\Delta D_{mp} << \frac{c}{B_m} \qquad (1) \ .$$

  Where $\Delta D_m = \| \mathbf{E}_m \mathbf{R}_p \| + \| \mathbf{R}_p \mathbf{A} \| - \| \mathbf{E}_m \mathbf{A} \|$ is the distance difference of arrival between direct-path and *p*-path of the *m*-transmitter, B_m the bandwidth and *c* the light speed.
- **The non-coherent case** : The transmitter bandwidth is larger than the inverse of time difference of arrival between direct-path and multi-path.

The following table shows the limit distance of ΔD_m to obtain coherent path with respect to the bandwidth of the transmitter.

B_m (MHz)	**300kHz**	**1MHz**	**10MHz**
Limit distance	< 246m	< 74m	< 7m

Table 1- Limit distance to obtain coherent path

In that way AOA HR algorithms, adapted to the coherent case, are the sub-family of ML algorithms (Maximum Likelihood)[16] -[18] . When the sources are not coherent the best algorithm is MUSIC[15] . The AOA technique is chosen adaptively to the coherent sources . Figure 10 shows that the choice of AOA algorithms depends on the MUSIC criterion

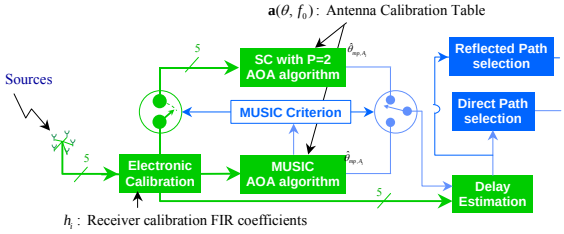

Figure 10- Mono-station Adaptive Elementary AOA technique

The previous Figure shows that AOA technique needs Calibration Table with steering vectors $\mathbf{a}(\theta, f_0)$ for all directions θ and frequencies f_0. In the case of GALILEO the values of f_0 are 1183MHz, 1266MHz and 1566MHz for the channels E5, E6 and L1 respectively. In practice the elementary AOA technique is applied on a multi-sensors signal of duration T_0. The AOA result is given from a signal of duration T with multiple(T/T_0) elementary AOA. After an AOA synthesis, the result associated to the *m*-transmitter is the main direction $\bar{\theta}_{m,A}$ and the associated standard deviation $\sigma_{\theta_m,A}$.

Location algorithm

The location technique with the stations **A**, **B** and **C** uses the results $\left(\bar{\theta}_{i,A}, \sigma_{\theta_i,A}\right)$, $\left(\bar{\theta}_{j,B}, \sigma_{\theta_j,B}\right)$ and $\left(\bar{\theta}_{k,C}, \sigma_{\theta_k,C}\right)$ $\left(1 \le i, j, k \le M\right)$ at the output of the AOA synthesis. One of the problem is to find indices $\left(i_m, j_m, k_m\right)$ associated to the same transmitter. On the assumption that $\left(\bar{\theta}_{i,A}, \sigma_{\theta_i,A}\right)$

and $\left(\overline{\theta}_{j,B}, \sigma_{\theta_{j,B}}\right)$ are associated to the same transmitter, the location is estimated at $\mathbf{E}_{ij}$ with an uncertainty ellipse of parameters (δD_{ij}^{min}, δD_{ij}^{max}, φ_{ij}) as represented on the following figure.

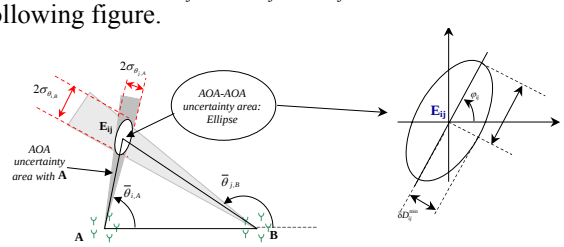

Figure 11- Location technique with the stations A and B

The location $\mathbf{E}_{ij}$ is the intersection between the straits of direction $\overline{\theta}_{i,A}$ and $\overline{\theta}_{j,B}$ and the parameters of the uncertainty ellipse are estimated from the standard deviation $\sigma_{\theta i,A}$ and $\sigma_{\theta i,B}$. The location $\mathbf{E}_{ij}$ is a true location when the location $\mathbf{E}_{ik}$ (intersection between the straits of direction $\overline{\theta}_{i,A}$ and $\overline{\theta}_{k,C}$) and $\mathbf{E}_{jk}$ (intersection between the straits of direction $\overline{\theta}_{j,B}$ and $\overline{\theta}_{k,C}$) are inside the uncertainty ellipse of parameters (δD_{ij}^{min}, δD_{ij}^{max}, φ_{ij}). When the indices (i, j, k) are associated to the same transmitter by the previous technique, the location $\mathbf{E}_m$ and the associated uncertainty ellipse of parameters (δD_m^{min}, δD_m^{max}, φ_m) are estimated from ($\overline{\theta}_{i,A}$, $\sigma_{\theta i,A}$),($\overline{\theta}_{j,B}$, $\sigma_{\theta j,B}$) and ($\overline{\theta}_{k,C}$, $\sigma_{\theta k,C}$) with a mean square algorithms.

Simulations

The simulations consider the case of 3 AOA stations (IOS positions in green in
) in presence of one interference located in $\mathbf{E}_1$ and one reflector located at $\mathbf{R}_1$ (in blue in
). The *i-th* scenario depends on the location $\mathbf{E}_1$ of the interference (in red with the index ($1 \leq i \leq 7$)in
). Figure gives the location results of the interference located at $\mathbf{E}_1$(200+100(*i*-1) meters, 1000-200(*i*-1) meters) and the reflector at $\mathbf{R}_1$(300meters,-100meters). The accuracy of the interference is between 2 meters and 20 meters and depends on the location of the interference.). Figure gives the location results of the interference located at $\mathbf{E}_1$(200+100(*i*-1) meters, 1000-200(*i*-1) meters) and the reflector at $\mathbf{R}_1$(300meters,-100meters). The accuracy of the interference is between 2 meters and 20 meters and depends on the location of the interference.

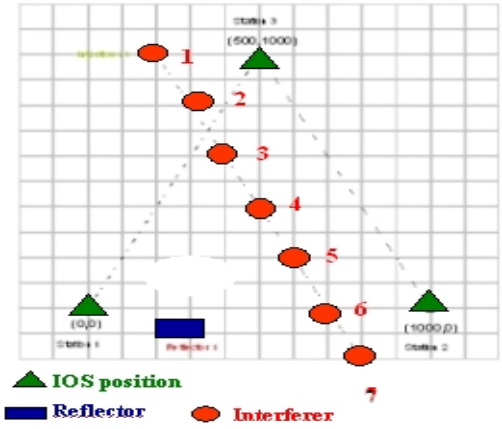

Figure 12 - Interferer and reflector positions

		Real Position	Detected Interferers	Detected Reflectors
1	Scenario 3-1-1	(200,1000) (300,-100)	(200, 996.37)	(303.12, -96.84)
2	Scenario 3-1-2	(300, 800) (300,-100)	(309.58, 803)	(297.02, -95.81)
3	Scenario 3-1-3	(400, 600) (300,-100)	(396.32, 591.54)	(223.96, -93.67)
4	Scenario 3-1-4	(500, 400) (300,-100)	(505.65, 397.69)	(311.11, -105.79)
5	Scenario 3-1-5	(600, 200) (300,-100)	(593.42, 205.53)	(363.7, -125..37)
6	Scenario 3-1-6	(700, -000) (300,-100)	(717.44, 1.52)	(303.98, -1.71)
7	Scenario 3-1-7	(800, -200) (300,-100)	(808.66, -217.43)	-

Figure 13 – Location results with Interferer and reflector

VI. TEST BED

The general synopsis of the test bed shows below the different equipment used during the field trial.

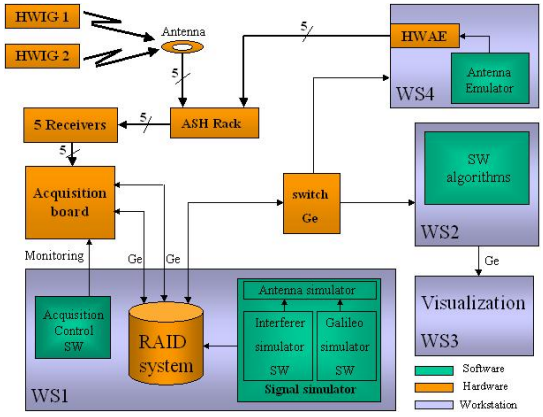

Figure 14 – Test Bed Synopsis

The test bed is composed by:

- A circular array with five dipole working in the bandwidth 500 MHZ to 3 GHz
- A five matched channels receiver able to manage 40 MHz of bandwidth
- An acquisition system of five raw analogue input signals that will be used for analogue-digital conversion of antenna sensors or hardware simulators outputs. This acquisition system will store a 4 seconds snapshot of signal on the 4 GBytes RAM memory available on the board.
- A workstation 1 (WS1) used to control the acquisition system and store the acquisition files in the RAID disks.
- A workstation 2 (WS2) used to run and compute all the algorithms software allowing the detection, mitigation and isolation of the interfere sources of the Galileo signals. These algorithms work on the data received from the WS1.
- A workstation 3 (WS3) used to run the visualization of the interferer positions and characteristics on the map of the area.

- A workstation 4 (WS4) used to transmit a signal through the acquisition system to compute the calibration filter, in order to equalize the level and the phases of each channel.

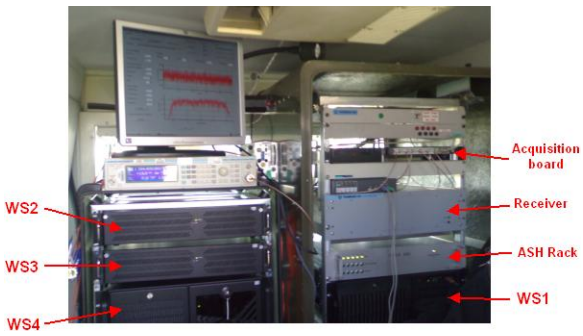

Figure 15 – Equipment inside the IOS test bed vehicle

This equipment was embedded in a four-wheel drive van as shown by the following picture.

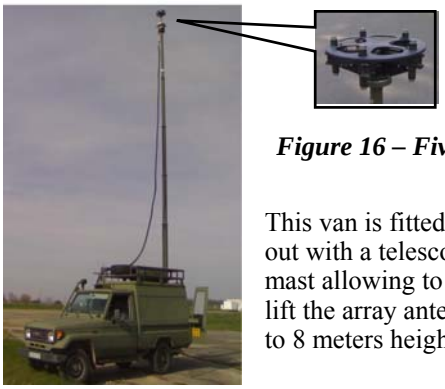

Figure 16 – Five Sensors Array

This van is fitted out with a telescopic mast allowing to lift the array antenna to 8 meters height.

Figure 17 – IOS Test Bed Vehicle and Reception Array

An interferer transmitter system allows during the lab and synthetic trials on site to generate different waveforms as CW, narrow or wideband noise signals, no or filtered linear modulations, continuous or pulsed signals. The antenna simulator software implemented on the WS1 computer generates these signals.

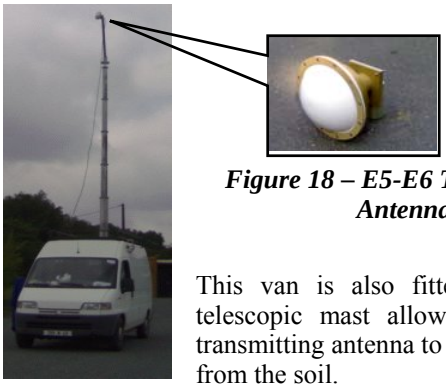

Figure 18 – E5-E6 Transmitting Antenna

This van is also fitted out with a telescopic mast allowing lifting the transmitting antenna to 8 meters height from the soil.

Figure 19 – Interferer Van and Transmitting Antenna

The antenna simulator is able to generate Interferer signals as previously described, Reflected interferer signals, Galileo signals in the E5a, E5b, E6 and L1 bandwidth and thermal noise on five sensors in order to simulate the MAGIC array antenna. The X, Y, Z coordinates of each source are tuned by the operator through the MMI.

A reflector system was implemented in order to test the location algorithm in situ. The reflector system is composed by:

- A first YAGI antenna pointed in the interferer Transmitter direction and receiving the interferer signal (A).
- An amplifier (Gain) transmitting the receiving signal (A) on a 25 meters cable towards the Re transmitter.
- A second YAGI antenna pointed in the direction of the IOS that retransmit the previous received signal (A).

This equipment was used in order to test the location algorithms with coherent or not coherent multi path simulated environment.

Figure 20 – Reflector System

VII. SYNTHETIC TRIALS ON SITE WITH SIMULATED INTERFERENCES

Synthetic interferer trials have been realized in May 2007 around Cholet (F).The results got are presented below.

Detection

Field trials have been carried out to analyse the behaviour of the Detection and Mitigation Algorithms in several different situations. The analysis concerning the detection and mitigation processing reported in this paper is based on the data recorder at the Le Verdon Lake (near Cholet, France). First of all the scenario under test has been prepared putting on the field two different interference sources (red bullets in the Figure 21

Figure 21 – Le Verdon Lake Field Trials Scenario

Then the interferers have been recorded in three different positions by the MAGIC Test Bed (green bullets in figure

Figure 21). Finally the spectrum of the signal received has been extracted obtaining a diagram like that shown in Figure 22. In this particular case the following interfering signals have been generated: (i) a pulsed signal with PRF = 5KHz, centred at -10 MHz; (ii) a sweep, with start frequency at 7 MHz and stop frequency at 13 MHz. Some spurious signals are also present: (i) a spurious CWs at 0 MHz; (ii) other minor scattered spurious. The interfering signals have been correctly detected and classified.

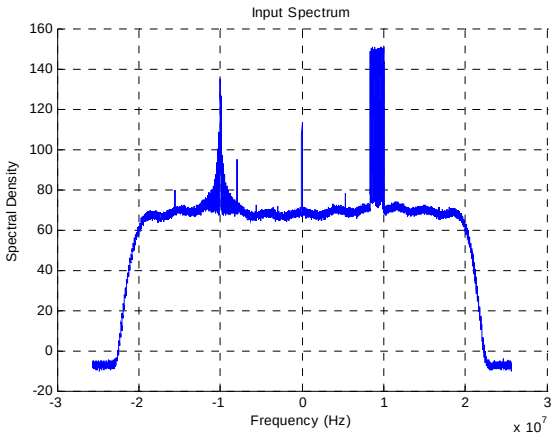

Figure 22 – Received Spectrum (Le Verdon)

Mitigation

As far as the mitigation process is concerned, the FDIM algorithm performs as expected apart considering the unwanted spurious CWs, already present in the calibration noise. The FDIM results are shown in figure 23 (original signals in blue, mitigated signals in red): the pulsed interference is attenuated by 50 dB and the sweep is attenuated by 60 dB. Also some unwanted spurious signals have been attenuated at the threshold level.

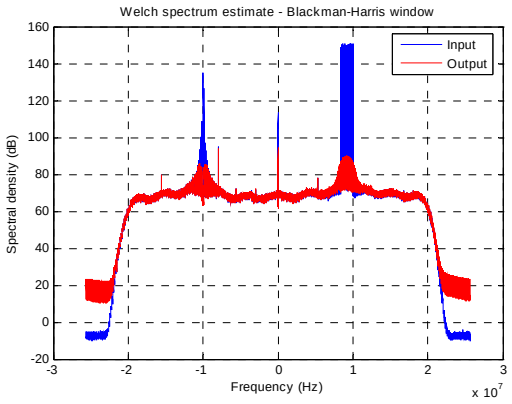

Figure 23 – FDIM Performances (Le Verdon)

In Figure24, it is displayed the result of SDIM, as a spectrum overlapped to the input spectrum (original signals in blue, mitigated signals in red). The unintentional interferences have not been attenuated since not detected. The performances are satisfying also if limited by DOA estimation errors: (i) Sweep (strongest) AoA Azimuth Error: 1.93°; (ii) Pulsed (weakest) AoA Azimuth Error 0.92°.

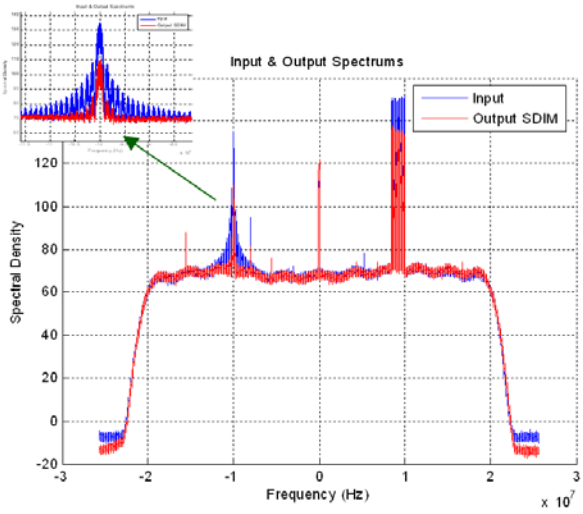

Figure 24 – SDIM Performances (Le Verdon)

Isolation

Different type of scenarios have been planed to test the demonstrator:

- Transmission of one interferer.
- Transmission of one interferer and presence of one reflector.
- Transmission of two simultaneous interferers

One interferer and one reflector case

This scenario took place in Noues's lake, in east of Cholet. One interferer and one reflector were positioning around the lake and the transmitted interference was a filtered QPSK in the E5 bandwidth.

	Measurement point			Interferer	
	Station 1	Station 2	Station 3	Real position	Estimated position
X (m)	0	-308.59	-260.7	141.74	172.72
Y (m)	0	125	637.47	655.1	638.72
Real angle of arrival (deg)	77.79°	49.65°	2.5°		
Estimated angle of arrival (deg)	75.38°	46.21°	0.7°		
Error of angle (deg)	2.41°	3.44°	1.8°		
				Reflector	
X (m)	0	-308.59	-260.7	-224.68	-223.29
Y (m)	0	125	637.47	303.34	287.66
Real angle of arrival (deg)	126.52°	64.8°	276.15°		
Estimated angle of arrival (deg)	127.81°	62.3°	276.09°		
Error of angle (deg)	1.29°	2.5°	0.06°		

Table 1: Interferer and reflector location results

The results got show errors on DoA less than 3.5° and a resulting error on the X, Y position less than 5%.
The satellite picture presents the position of each station and the location of the interferer in the upper right part and the reflector in the middle left part. In this example, the interferences were transmitted in E5. The distances between interferer and the stations were around 500 meters. The two ellipses on each bottom side of the

previous picture is the theoretical possible location error area. The red arrow shows the distance between the real and estimated positions of the two interferers. The error of localization was 35 meters for the interferer and 16 meters for the reflector. (error < 5%).

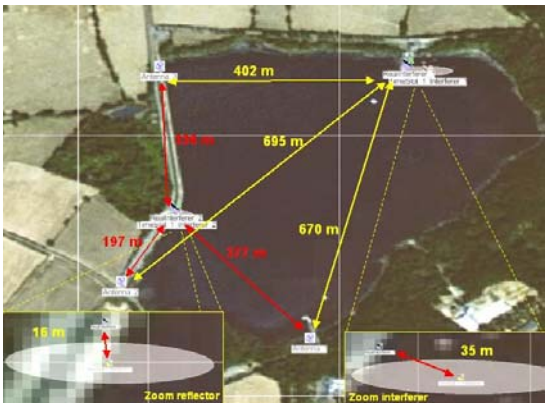

Figure 25 – Interferers Reflector and Antennas Position on the Noue's Lake Map

Two simultaneous interferers case

	Measurement point			Interferer 1	
	Station 1	Station 2	Station 3	Real position	Estimated position
X (m)	0	-729.09	-202.55	473.7	477.07
Y (m)	0	-458.25	-1748.98	-376.8	-414.41
Real angle of arrival (deg)	321.5°	3.87°	63.76°		
Estimated angle of arrival (deg)	319.51°	1.8°	63.17°		
Error of angle (deg)	1.99°	2.07°	0.59°		
				Interferer 2	
X (m)	0	-729.09	-202.55	-530.33	-530.98
Y (m)	0	-458.25	-1748.98	17.62	40.6
Real angle of arrival (deg)	178.1°	67.33°	100.51°		
Estimated angle of arrival (deg)	174.94°	67.15°	100.75°		
Error of angle (deg)	3.16°	0.18°	0.24°		

Table 2: Two interferers location results

All the distances between the jammers and the measurement stations are ranged between 500 meters and 1.7 kilometres, the localization is correct- because the error of estimation is only 38 meters for the first interferer and 23 meters for the second interferer.
The average of error of angle of arrival is around 2 degrees according the measurement and the real position of each station. The following satellite picture shows the positions of the two interferers, and the three antennas around the Verdon Lake.

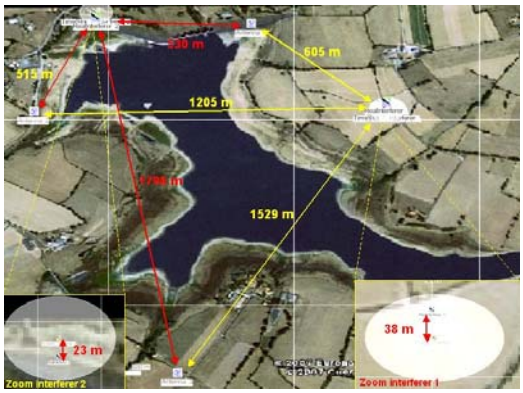

Figure 26 – Interferers and Antennas Position on the Le Verdon Lake Map

The error on the positions is also less than 5%.

VIII. TRIALS ON SITE WITH EXISTING INTERFERENCES

These following tests have been aimed at evaluating MAGIC performance on location in the presence of real interferences.

Figure 27 – Primary Radar and DME

To realize the trials, the measurements have been done on a civilian radar, such as primary radar or a DME (Distance Measurement Equipment). in July 2007 around Paris (CDG) and Orléans (F).

These two equipments are considered as Galileo interferers in the E5 bandwidth. The results got are presented below.

Detection

Data has been recorded in several locations. Among them the scenario recorded in Dammartin has been taken as representative sample in this paper. A frequency representation of the signal received in E6 Galileo band is given in Figure 28. The CW at 0 MHz is a spurious signal already present in the noise mask whereas the second peak near -5MHz is the DME signal.

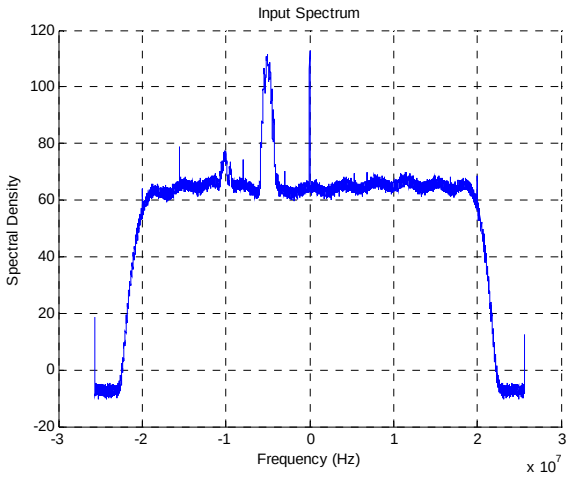

Figure 28 – Received Spectrum (Dammartin)

The interference has been correctly detected and the coarse estimations of the central frequency and bandwidth are given. The signal has been classified as generic signal being the signal of the DME equipment a pulse to pulse-staggered signal, which provides a variable

PRF whereas the classification algorithm can only classify signals having a constant PRF. The spurious at 0 MHz has not been detected because already present in the noise mask.

Mitigation

Next Figure 29 shows the effect of the FDIM algorithm on the received signal. As it is possible to note the DME signal has been attenuated about 40 dB.

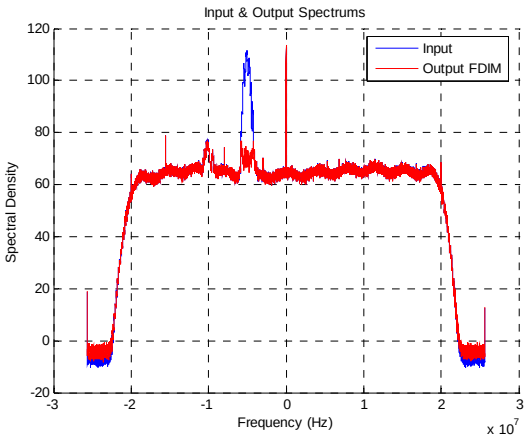

Figure 29 – FDIM Performances (Dammartin)

Localization of primary radar

The localization of primary radar has been done at Dammartin-en-Goële near Charles De Gaulle airport. This kind of radar transmits a double pulse with two frequencies. The frequency of the first pulse is 1250 MHz and 1255 MHz for the second.

	Measurement point			Radar	
	Station 1	Station 2	Station 3	Real position	Estimated position
X (m)	0	-1489.92	-1559.84	395.71	457.55
Y (m)	0	-3409.08	-1297.03	-2142.11	-2249.21
Latitude (DMS)	49°5'3.15"	49°3'12.9"	49°4'21.21"	49°03'53.68"	
Longitude (DMS)	2°38'36.74"	2°37'23.21"	2°37'19.73"	2°38'56.27"	
Real angle of arrival (deg)	280.47°	33.9°	336.63°		
Estimated angle of arrival (deg)	281.5°	-	334.73°		
Error of angle (deg)	1.03°	-	1.9°		

Table 3 -- Primary radar location results

The results showed that the signal at the second measurement was too weak to deliver an angle of arrival. The reception antenna was behind a hill, and it wasn't possible to look directly at the primary radar. However, two measurements are sufficient to deliver a location when there is only one jammer.

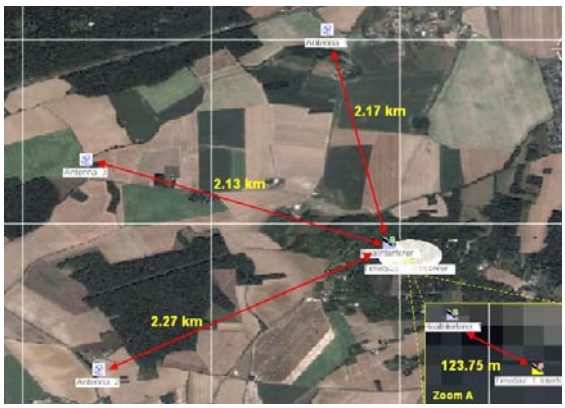

Figure 30 – Radar and Antennas on the Local Map

The distance between the primary radar and the measurement station was around 2 kilometres. The error between the real position of the radar and the estimated position is approximately 123 meters (zoom shows on the right bottom side) that represents around 5% of error.

Localization of DME

Localization of several DME have been done at about 100 km in the south west of Paris. The trial presented below took place at Châteaudun. The equipment located is a DME transmitted a double pulse at 1195 MHz.
The following table shows the results got on this interferer.

	Measurement point			DME	
	Station 1	Station 2	Station 3	Real position	Estimated position
X (m)	0	-2503.74	-5048.42	-2835.29	-2949.85
Y (m)	0	-1777.55	-1910.57	1370	1473.35
Latitude (DMS)	48°2'36.59"	48°1'39.11"	48°1'34.81"	48°03'20.9''	
Longitude (DMS)	1°24'48.58"	1°22'47.51"	1°20'44.46"	1°22'31.4"	
Real angle of arrival (deg)	154.21°	96.01°	55.99°		
Estimated angle of arrival (deg)	153.16°	98.28°	57.88°		
Error of angle (deg)	1.05°	2.27°	1.89°		

Table 4 – Results of the DME location

The particularity of this trial is the position of each station of measurement. The graphic below shows that they are dispersed in 18 km² area (~ 6*3 kms). The measurement points form more a little curve in south of DME than a classical triangle that is the best figure for triangulation measurements Moreover, distances between the interferer and the measurement station are much bigger than those in previous test because they are at least 3 kilometers.
In spite of this no optimal configuration to achieve the best localization results, the average error of angle of arrival is less than 2 degrees and the error of positioning between the real position and the estimated position is around 150 meters that equal approximately to 5% of error.

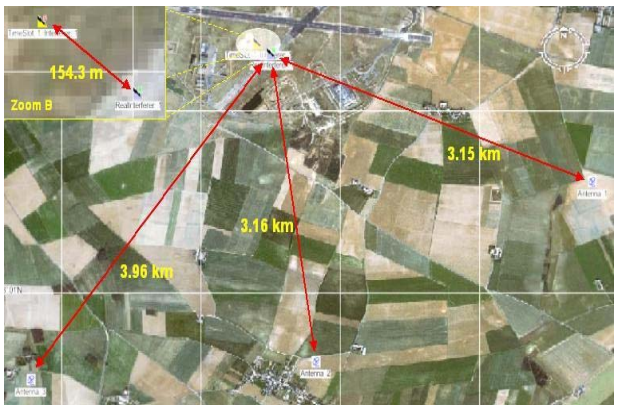

Figure 31 – DME and Antennas Position on the Local Map

IX. GIMS (GALILEO INTERFERER MANAGEMENT SYSTEM)

This section briefly reviews the concept of GIMS in order to complete the architecture envisaged for the target LAAS plus the GIMS structure. The GIMS is the strategy proposed by the MAGIC Project to face the problems caused by the presence of interfering signals.
This system will be able to deliver the position X, Y, Z of fix or mobile interferers.
Two kinds of interferers might be considered as:

- Intentional interferer that would be pulsed or continuous, wide , narrow bandwidth or constant wave. The signal would be also noise, Spread Spectrum, OFDM or classical modulation …
- Unintentional interferers as plane radars, wind profilers, DME, TACAN, … and all the existing equipment used by the army, the civilian airports, the meteorologist, ….

This family of interferers will be able to transmit and jam the bandwidth 1.1 to 1.65 GHz that include the Galileo, GPS, GLONASS positioning system signals.
In case of intentional interferers the system can be carried by a plane, helicopter, a stopped or mobile van ....
The following figure shows the typical architecture of the LAAS and the GIMS put side by side.

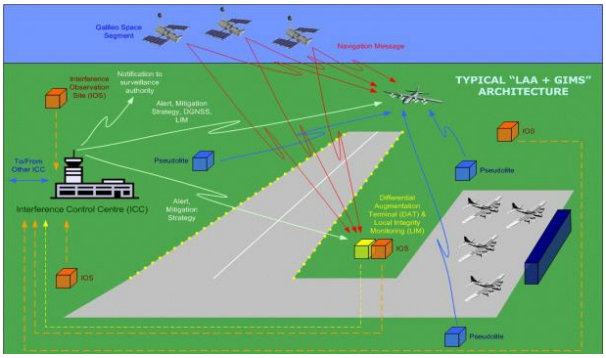

Figure 32 – LAA and GIMS

This system is able to manage three main functions:

- Interference Detection and Classification: to discover the presence of interfering signals affecting the managed area and to determine their main characteristics;
- Interference Isolation: once the presence of the interference has been detected, to find their exact position;
- Interference Mitigation: to provide to the GR all the parameters necessary to put in force a mitigation strategy (which is not part of the GIMS but it is studied in the MAGIC project to be implemented inside the GR);

The GIMS is based on the following main equipments:

- **IOS (Interference Observation Site)**: devices able to detect the presence of interfering signals and to provide information on them like frequency, bandwidth, AOA and so on;
- **ICC (Interference Control Centre)**: that receives the information from each IOS and extracts the position of each interfering signal associating it with its main characteristics. Furthermore it also provides: (I) A Signal Alert to warn the area about the interference presence; (II) The Notification to the Surveillance Authority; (III) The Mitigation Strategy to each GR belonging to the controlled area and including those of the LAA.

CONCLUSIONS

The main goals of the MAGIC project were:

- Complete the knowledge about the (un)intentional interferers
- Realize a software scenario simulator in order to predict the efficiency of the interferer detection mitigation and location algorithms.
- Study, develop and test in labs detection, mitigation and isolation algorithms robust to multi path situations.
- Realize a test bed allowing trials in situ on the basis of a 4 WD fitted with a reception antenna at 8 meters height
- Validate the algorithms and the isolation concept on synthetic and real interferers in the Galileo bandwidth E5, E6, L1.

The MAGIC results achieved on the previous goals:

Unintentional interferers

The knowledge about unintentional interferers has been completed by providing an interference analysis based on Real measurements, information from available technical sources and cooperation with the communications authority. Further analysis on real existing interferers in the Galileo bands has been obtained during the MAGIC field trials and the measurements during the travel to these locations.
The analysis showed that the most detections occurred in the E5 and E6 bands, less detections were noted in the L1 band. Two airports (Milan and Paris Orly) were investigated for interference in the Galileo bands but only at one airport (Milan) significant interference was found.

Type of interferers available on the MAGIC test bed

The previous objectives have been successfully delivered with regards to the following type signals:

i) Synthetic interferers transmitting in E5, E6, L1 bandwidth as :

- constant frequency, narrow or wide band signals
- classical modulation as QPSK not or filtered,
- noise, continuous wave or pulsed signals

ii) Real interferers as:

- DME transmitting in E5 bandwidth
- Primary radar of civilian aviation transmitting in E6 bandwidth

Detection and classification

The signals listed above have been successfully detected after the calibration carried out on the input noise. The detection and classification processing also correctly provided the first set of coarse parameters estimation concerning:

- The narrow band versus wideband classification;
- The bandwidth of each detected signal;
- The central frequency of each detected signal;
- The SNR ratio of each detected signals;

Moreover the specific algorithms developed to recognize the pulsed signals with constant pulse width and PRF and the sweeping signals also correctly classified these kind of signals providing a fine estimation of the following parameters:

- A classification flag identifying the type of the signal;
- The pulse width of pulsed signals (in case of pulsed signals with constant pulse width and constant PRF);
- The PRF of pulsed signals (in case of pulsed signals with constant pulse width and constant PRF);
- The sweeping rate of sweeping signals (in case of sweeping signals);
- The initial frequency of sweeping signals in the observed time slot (in case of sweeping signals);

The parameters provided by the detection and the mitigation algorithms to correctly set them configuration have exploited classification processing.

Mitigation

The signals listed above have been processed by the mitigation algorithms obtaining satisfying result. The four kinds of algorithms developed (FDIM, SDIM, TFDIM and STFDIM) have correctly worked exploiting their peculiar characteristics:

- The FDIM and TFDIM correctly excised the part of the Galileo signal bandwidth corresponding to the frequency position of the interferences exploiting the indications provided by the classification algorithms;
- The SDIM correctly excised the directions of arrival of the interfering signals putting nulls in those directions according to the accuracy of the direction provided by the isolation processing;
- The STFDIM correctly excised the interfering frequencies keeping the beam forming toward the default direction of the Galileo signals;

These algorithms must be used at the GR side and implemented inside the receiver section. They covers all the aspects of the mitigation approaches being developed and tested in the three domains T (Time), F (Frequency) and S (Space). In some case they overlap to each other so the final algorithm to implement in a commercial GR should be extracted from them according to an analysis about their synergies and performances.

Isolation

All the signals listed above were successfully used in order to obtain the Direction of Arrival of the transmitter. The association between two or three DoA measurements has allowed to got the exact position of the interferer with less than 7% of error on the distance between the IOS and the intentional interferer (synthetic transmission) or the unintentional interferer (DME or primary radar).
The isolation was successfully realized in case of

- One interferer
- Two uncorrelated interferers
- One interferer and one reflector (coherent or not coherent path)

In all these situations and in particular with one reflected path the real direction of the sources was delivered.
The number of sensors of the array limits the number of uncorrelated sources and/or coherent paths. Typically the MAGIC circular array composed of N=5 sensors limits the number of sources to two, according to the following approximate equation : ([N-1]/ 2). Thus considering this last argument only two sources were used during these trials.

X. REFERENCES

[1] Galileo Signal in Space ICD, ID/GAL/0258/GLI, Issue 8.0, 21 October 2004.

[2] H. Urkowitz – Energy Detection of Unknown Deterministic Signals – Proceedings of the IEEE, Vol.55, No.4, April 1967.

[3] H.K.Mardia – New Techniques for deinterleaving of repetitive sequences – IEE Proceedings, Vol 136, No. 4, August 1989.

[4] B.Boashash – Estimating and interpreting the instantaneous frequency of a signal (part1: fundamentals) – Proceedings of the IEEE, Vol 80, No. 4, April 1992.

[5] B.Boashash – Estimating and interpreting the instantaneous frequency of a signal (part2: algorithms and applications) – Proceedings of the IEEE, Vol 80, No. 4, April 1992.

[6] T.J.Abatzoglou – Fast maximum likelihood joint estimation of frequency and frequency rate – ICASSP 86 Tokio, CH2243-4/86/0000-1409, 1986 IEEE.

[7] H.Steyskal – Synthesis of antenna pattern with prescribed nulls – IEEE Transactions on antennas and propagation, Vol. ap-30, no. 2, March 1982.

[8] J.W.Ketchum, J.G.Proakis – Adaptive algorithms for estimating and suppressing narrow-band interference in PN spread spectrum systems – IEEE Trans on communications, Vol. COM-30, no. 5, May 1982.

[9] H.V.Poor, L.A.Rusch – Narrowband interference suppression in spread spectrum CDMA – IEEE personal communications magazine, Third quarter 1994, pp.14-27.

[10] L.B.Milstein – Interference rejection techniques in spread spectrum communications – Proceedings of the IEEE, Vol. 76, no. 6, June 1988.

[11] G.J.Saulnier – Suppression of narrowband jammers in a spread-spectrum receiver using transform-domain adaptive filtering – IEEE journal on selected areas in communications, Vol. 10, no. 4, May 1992.

[12] X.Chen, W.Guo, Y.Zheng – Frequency domain interference suppression in a DSSS system – IEEE 2002 international conference on communications, circuits and systems and West Sino Expositions, 2002.

[13] A. Papoulis – Signal Analysis – McGraw Hill.

[14] Harry L. Van Trees – Optimum Array Processing – Part IV of Detection, Estimation, and Modulation Theory, John Wiley & Sons, Inc., New York, 2002.

[15] RO.Schmidt. A signal subspace approach to multiple transmitter location and spectral estimation, PhD thesis, Stanford Universoty, CA, November 1981.

[16] B.Ottersten, M.Viberg, P.Stoica and A.Nehorai Exact and large sample maximum likelihood techniques for parameter estimation and detection in array processing. In S.Haykin, J.Litva and TJ.Shephers editors, Radar Array Processing, chapter 4, pages 99-151. Springer-Verlag, Berlin 1993.

[17] P. Larzabal Application du Maximum de vraisemblance au traitement d'antenne : radio-goniométrie et poursuite de cibles. PhD Thesis, Université de Paris-sud, Orsay, FR, June 1992.

[18] A.Ferréol, E.Boyer and P.Larzabal A low cost algorithm for some bearing estimation methods in the presence of separable nuisance parameters. Electronics Letters, 40 (15) : 966-967, July 2004.